Am J Cancer Res 2015;5(1):32-51
www.ajcr.us /ISSN:2156-6976/ajcr0002563

Original Article

Prediction of non-small cell lung cancer metastasis-associated microRNAs using bioinformatics

Rong Wang, Xiao-Feng Chen, Yong-Qian Shu

Department of Oncology, The first affiliated Hospital of Nanjing Medical University, Nanjing 210029, China

Received September 16, 2014; Accepted November 10, 2014; Epub December 15, 2014; Published January 1, 2015

Abstract: Distant metastasis is one of the most common causes for failure in treatment of advanced NSCLC, and it is a key factor to determine the patients' prognosis. This study aims to screen the microRNAs associated with non-small cell lung cancer metastasis, so as to provide theoretical basis for investigating their roles in non-small cell lung cancer metastasis. In this study, the fluorescent transfected human non-small cell lung cancer cell lines H460 developed tumors subcutaneously, which were then *in situ* transplanted into the left lung of nude mice to obtain the tissue specimens of primary tumor and metastatic tumor. The differentially expressed microRNAs associated with non-small cell lung cancer metastasis were identified using the microRNA microarray and real-time quantitative polymerase chain reaction (RT-PCR) analysis, and bioinformatics analysis of the microRNAs was performed. The microarray analysis results revealed that 17 microRNAs with up-regulated expression and 7 with down-regulated expression between the non-small cell lung cancer metastatic primary loci and the non-metastatic primary loci (Group A), while 20 microRNAs with up-regulated expression (ratio > 1.5 times, $P < 0.05$) and 16 with down-regulated expression (ratio < 0.65 times, $P < 0.05$) between the non-small cell lung cancer metastatic loci and the metastatic primary loci (Group B). RT-PCR validation and bioinformatics analysis of some microRNAs identified 2 microRNAs with up-regulated expression, miR-10b and miR-144, and 3 microRNAs with down-regulated expression, miR-9, miR-31 and miR-34b in Group A; and 4 microRNAs with down-regulated expression, miR-25, miR-92a, miR-202 and miR-326 in Group B, which may be mediated by transcription factors activator protein 1 (AP-1), p53, STATs and NF-κB, regulate cell development, proliferation and cycle, DNA and RNA metabolism and signal transduction pathway, and promote tumor growth and metastasis through the effects on target genes like *RARβ*, *RASSF1* and *E2F-1*. In conclusion, there are differences in microRNA expression between the non-small cell lung cancer metastatic and non-metastatic tissues, which provides experimental basis for exploring the mechanism of non-small cell lung cancer metastasis and provides a potential idea for molecular diagnosis and treatment, as well as prognosis.

Keywords: Non-small cell lung cancer, metastasis, microRNA, microarray, nude mouse model, target gene

Introduction

The incidence of lung cancer ranks second among malignant tumors worldwide, but it is the leading cause responsible for death of malignant tumors. Non-small cell lung cancer (NSCLC) is the most common, accounting for about 80% of all lung cancer. The disease has a low rate of early diagnosis, and local and distant metastases are detected in 75% of the cases while clinically diagnosed. Lymph node metastasis is an important prediction index for clinical staging and prognosis assessment, which suggests high tumor malignancy and poor prognosis [1, 2]. Mountain and Dresler [2] investigated the relationship between lymph node metastasis and post-surgical survival, and revealed that lymph node metastasis indicated high tumor malignancy and poor prognosis, the patients usually did not die of primary loci-induced symptoms, but die of the related complications caused by metastatic loci, such as brain metastasis, the compression and infringement of mediastinal lymph node metastasis on adjacent organs, or the malignant pleural effusion caused by pleural metastasis. Currently, a great deal of advances has been achieved in molecular pathogenesis of NSCLC. However, only 1/8 of the patients are cured at an early stage, while other cases fail to be cured due to distant metastasis [3]. Distant metastasis is one of the most common causes for fail-

ure in treatment of advanced NSCLC, and it is a key factor to determine the patients' prognosis. It is therefore, of great importance to explore the mechanism of NSCLC metastasis and the strategy to block the metastasis of the disease.

Multiple mechanisms are involved in tumor metastasis, which is an indicator for tumor malignancy. Tumor cells firstly bind with extracellular matrix adhesion protein. Subsequently, secreted proteases hydrolyze the matrix and migrate from the primary loci. Some cancer cells penetrate the endothelial basement membrane into the lymphatic vessels and blood vessels, migrate to new organs via the circulation, attach to vascular endothelial cells and stick out to form metastatic loci. Many mechanisms including factors-promoting mechanism, signal pathway mechanism, adhesion mechanism, extracellular matrix degradation mechanism, metastatic gene regulation mechanism, are involved in the process of metastasis. Target of tumor metastasis is the current research focus. With the deepening of research in microRNA (miRNA), it is indicated that post-transcriptional regulation is widely present in organisms. miRNAs are single-strand small-molecule RNAs with 21-24 nucleotides, which are involved in cell proliferation, differentiation, apoptosis, embryo development, morphogenesis and disease occurrence during the process of cell growth and development. It is estimated that about 1/3 of human genes are mediated by miRNAs, which negatively regulate gene expression by interfering with mRNA translation [4]. Each miRNA has many target genes, while several miRNAs may regulate the same gene. About 50% of the identified miRNAs are located at tumor-associated fragile sites in a genome [5]. Some miRNAs can function as oncogenes like miR-21, miR-155 and miR-17-92 gene cluster, and tumor suppressors such as miR-125b-1, miR-15a, miR-16-1, miR-143 and miR-145 [6]. During different stages of NSCLC occurrence and development, whether the invasion and metastasis of the disease is mediated by miRNAs remains unknown. It is assumed that the differentially expressed miRNAs between the metastatic primary loci and non-metastatic primary loci suggest the regulation of the beginning of metastasis, and the differentially expressed miRNAs between the metastatic loci and metastatic primary loci indicate the regulation of the metastasis.

To obtain the specimens of metastatic foci is critical to investigate the role of lung cancer metastasis-related miRNAs. Given that surgery is not recommended for the traditional stage IIIB-IV patients with NSCLC classified according to the taxonomy of cancer staging (TNM) system, it is difficult to obtain the specimens of metastatic foci. Although the NSCLC cases with stage earlier than IIIA are able to undergo surgery, the need of standard pathological examinations in clinical practices greatly limits the collection of the specimen of metastatic lymph node used for laboratory experiments, leading to the entry of previous studies with aim to explore the mechanism of lung cancer metastasis into a bottleneck. Therefore, the present study established animal models to obtain the specimen of lung cancer metastasis. Animal model is an important approach to conduct tumor study. Previously, nude mouse models of subcutaneous transplantation of lung cancer have been widely used, however, distant metastasis is rarely observed in this model. Since 1990s, the orthotopic implantation nude mouse models of human tumors have been sequentially established, which present the growth and metastasis similar to the clinical characteristics of human tumors. Replication of animal models of human tumors is able to study the *in vivo* tumor occurrence and development, which provides experimental basis for demonstrating the mechanism of tumor metastasis. The development of molecular imaging makes the real-time non-invasive *in-vivo* imaging of small animal tumor models possible [7, 8]. Optical imaging, due to non-ionizing low-energy radiation, high sensitivity, no need of radioactive reagent and low cost of the imaging system, is particularly suitable for the research of small animal tumors. Green fluorescent protein (GFP), as a new generation of reporter gene, has been widely applied in the biomedical sciences. GFP-based *in vivo* fluorescence imaging can be used to reveal the cellular and molecular mechanisms of tumor occurrence and development. Yang *et al*. [9, 10] employed whole-body optical imaging system for real-time, non-invasive fluorescence imaging of GFP-expressing tumors, and recording the process of tumor metastasis. The whole-body optical imaging system is external and noninvasive, and it is very sensitive and rapid for detection of soft organs and bone metastatic cancer [9]. Currently, GFP-expressing tumors of the lung, prostate, melanoma,

colon, pancreas, breast, ovary, brain, and other organs have also been visualized externally by use of quantitative transcutaneous whole-body fluorescence imaging [11], and metastatic mouse model has been established (Anti-cancer Inc., http://www.metamouse.com/). Currently, the studies regarding metastatic mouse model mainly focus on tumor growth, there are few literatures regarding the tumor metastasis, and there are few studies reporting the NSCLC metastasis-related miRNAs using metastatic mouse models.

The present study used nude mice and large cell lung cancer cell lines H460 to establish orthotopic implantation animal models of lung cancer [12], to stimulate the process of natural occurrence of NSCLC and obtain specimens for miRNA microarray analysis, with aim to identify some metastasis-related miRNA markers, so as to investigate the possible mechanisms preliminarily.

Materials and methods

Animals

Forty-six 4-6 weeks aged nude mice of the BALB/c strain (23 males and 23 females), each weighing 18-22 g, were purchased from the Nanjing General Hospital of Nanjing Military Command (Nanjing, China; Certificate No. SCXK-(Jun) 2007-012). All nude mice were raised and all experiments were conducted under SPF-level barrier system.

Tumor cell line

The frozen NCI-H460 cells were obtained from the American Type Culture Collection (ATCC number: HTB-177™), which were K-ras mutant and p53 wild human large cell lung cancer cell lines. The cells were cultured in RPMI-1640 (containing 10% fetal calf serum, 100 U/ml penicillin sodium and 100 μg/ml streptomycin) containing 10% fetal bovine serum at 37°C in an absolute humidity environment containing 5% CO_2.

GFP retroviral expression vector and transfection of tumor cells

At 24 h before transfection, the cell culture solution for H460 cells was changed (cell density of 20%-40%). The packaging cell line RetroPack™ PT67 (Clontech Laboratories Inc., USA) containing pLPCX-GFP retroviral expression vector was cultured in RPMI-1640 medium. At 24 h before transfection, the culture solution for PT67 cells was changed. When the density of PT67 packaging cells reached 80%-90%, cells were centrifuged, and the supernatant containing pLPCX-GFP vector was isolated, which was then filtrated through the nitrocellulose (NC) membrane with a mesh size of 0.45 μm to remove the bacteria. 100 μl of the supernatant (containing about 5×10^6 pLPCX-GFP) was added into the tumor cell culture plates (containing about 10^5-10^6 cells), and the tumor cells were transfected at at 37°C under a condition containing 5% CO_2. After 24 h of transfection, the culture solution was changed, and transfection was performed 3 times within 72 h to increase the transfection efficiency and copy. The transfection efficiency was observed under a fluorescence microscope. After 72 h of transfection, cells were harvested and transferred to the selective medium containing 200 μg/ml G418 (Gibco, USA), and the concentration of G418 gradually increased to 2000 μg/ml. The high-level GFP-expressing cells were screened in the 96-well plates, and the screened clones were mixed, and cultured in media without G418. The monoclonal screening of high-level GFP-expressing cells (H460-GFP) was done in G418 for 10 passages to ensure the stable expression of fluorescent protein.

Subcutaneous implantation of lung cancer cells on nude mice

About 1×10^6 H460-GFP cells were injected subcutaneously into the right side of the back of 2 nude mice. The post-seeding growth time was about 30-40 days. Many pre-tests for detection of cell cycle, fluorescence distribution curve and fluorescence rate by flow cytometry revealed that, when the diameter of the subcutaneous tumor of H460-GFP cells developed to 5-10 mm, cells grew well, almost during the logarithmic growth phase, and the fluorescence intensity became remarkably high, which were suitable for transplantation.

Orthotopic implantation of tumor tissues

The subcutaneous tumor was divided into tissue fragments measuring 1.0 mm × 1.0 mm × 1.0 mm in culture solutions, which were used as transplantation materials. The nude mice

were anesthetized with 2.5% isoflurane, and the anesthesia was sustained using 1.5% isoflurane. Transverse incisions of about 1 cm long were cut on the left chest between the fourth and fifth rib of the nude mice using surgical scissors under a surgical operating microscope at a magnification of 8x. The muscle between the fourth and fifth rib was cut, crossing the parietal pleura, and the lung tissues were exposed. Two H460-GFP tumor tissues were seamed on the surface of the lower lobe of the left lung tissue using the surgery sutures 8-0. In order to prevent the direct contact of the transplanted tissues with the thoracic cavity of nude mice, the surface of the lower lobe of the left lung was covered with the upper or middle lobe of the left lung. Finally, the thoracic cavity was closed using the surgery sutures 5-0. The entire open thoracotomy was not less than 1 min, and strictly followed aseptic principles.

Observation on animal experiment and collection of specimen

The survival and tumor growth of nude mice was observed every other day. *In-vivo* fluorescence imaging system is consisted of a stereo microscope (ZOOM645S, Jiangnan Yucheng Optical Instrument Co., Ltd, China) installed with 510-540 nm emission filters, charge-coupled device (CCD, Retiga Exi cooled Digital Color, QIMAGING, USA) and fluorescence excitation apparatus (LG-150-A, Nanjing Chaoteng Sci-Tech Development Co., Ltd, China) installed with 470-490 nm excitation filters. The imaging analysis software was the Image-Pro supplied by the MediaCybernetics Company (USA). The longitudinal diameter and transverse diameter of the primary tumor on the nude mice were measured under a fluorescence imaging system, and the tumor volume was calculated using the software Image-Pro, and the picture of tumor was photographed at a resolution of 1392 × 1040 pixels.

Plenty of pre-tests showed the occurrence of metastasis when the volume of the transplanted tumor on the thoracic cavity of nude mice grew to 150-200 mm^3, and the incidence of metastasis was about 70% when the tumor volume reached more than 1000 mm^3. The primary transplanted lesions were observed using the *in-vivo* fluorescence imaging system, and the size was measured every other day. The nude mice with extreme emaciation and poor activity were first sacrificed. According to the present study design, metastasis was detected in about half of the sacrificed nude mice. Therefore, in the present study, the nude mice were sacrificed at 2 weeks after orthotopic implantation, when the size of the primary transplanted tumor was about 200 mm^3, and most of the specimens collected were non-metastatic, and then a batch of nude mice were sacrificed every other week. On day 30 after orthotopic implantation, most of the left nude mice became remarkably emaciated, with significant reduction in activity, and outward expansion of the tumor mass on the left chest wall was observed by nude eyes, most of the tumors measured more than 1000 mm^3, and metastasis was detected in most of the dead mice. The thoracic cavity was opened, postmortem examination was performed, and the transplanted tumor on the left lung was recorded under the fluorescence imaging system, and the size and metastases of the contralateral lung, lymph node, liver, kidney, brain and bone of the primary tumor were observed. The primary and metastatic lesions of the tumors were quickly cut, and stored in liquid nitrogen at -196°C, 2-3 h later, they were stored at -80°C. Somo lesions were fixed in 4% formaldehyde.

Pathological examination

The lesion specimens were embedded in paraffin wax, cut into sections and stained with hematoxylin and eosin (HE) in the Department of Pathology of Jiangsu Provincial People's Hospital, and then the specimens were observed under a microscope, which was compared with the results revealed by the fluorescence imaging system.

RNA extraction

Four pairs of nude mice specimens with and without metastases (if the same nude mice had multiple metastases, all metastatic foci were considered as a specimen) were sampled from the aforementioned frozen tissues, including 4 primary lesions on non-metastatic nude mice, and 4 primary and metastatic lesions on metastatic nude mice. The frozen specimen were crashed, and then added with Trizol reagent (Invitrogen). After homogenating, RNA was extracted.

Assessment of RNA quality

The ratios of the absorbance at 260 nm (A_{260}) to the absorbance at 260 nm (A_{280}) of the RNA

solution were between 1.9 and 2.1, indicating no protein pollution. Two clear bands of 28S and 18S of total RNA were observed under the ultraviolet light following 0.75% formaldehyde denaturing agarose gel electrophoresis, suggesting no RNA degradation and DNA pollution.

Microarray hybridization

The miRCURY LNA™ (Locked Nucleic Acid) microRNA version 11.0 microarray (Exiqon, Denmark, http://www.exiqon.com/microrna-microarray-analysis) covered all miRNAs of humans, mice and rats in the miRBase 10.0 database (http://www.mirbase.org). Another 140 miRPlus™ probes were increased besides the miRBase database in the Exiqon microarray, and the number of probes reached 1300. The capture probes based on locked nucleic acid (LNA) technology were used, and each probe was repeated 4 times in the microarray, and the control probes included 12 small nuclear RNAs positive controls, 8 negative controls and 10 spike-in controls. miRNAs were labelled with Hy3™ or Hy5™ fluorescent groups using the miRCURY™ Array Power Labelling reagent kit to form fluorescent probes. A total of 13 microarrays were prepared for 12 specimens and their mixture, and the probes labelled with Phalanx™ heat shrinkable hybrid bags and the microarrays were hybridized under standard conditions.

Image collection and data analysis

The fluorescence intensity on the microarray was scanned using the Axon GenePix 4000B microarray scanner, and the original data were analyzed using the software GenePix pro version 6.0.

Screening of differentially expressed miRNAs

The background was removed from the signal value, and lowess and scale normalization was done. The ratio between groups > 1.5 times or < 0.65 times, and a P value < 0.05 revealed by t test indicated the miRNAs were differentially expressed. The ratio > 1.5 times was defined as up-regulation, while the ratio < 0.65 times was defined as down-regulation.

Bioinformatics analysis

The citation literatures were searched in NCBI-PubMed (http://www.ncbi.nlm.nih.gov/PubMed) using "non-small cell lung cancer" and "metastasis" as keywords. Based on over 5000 literatures, in combination with the recent studies regarding the mechanisms of NSCLC metastasis mediated by miRNAs, bioinformatics analysis of the differentially expressed miRNAs was performed.

Hierarchical clustering analysis

The expression values of the differentially expressed miRNAs were logarithm transformed, which were input into the hierarchical clustering algorithm. The distance chose "Pearson Correlation", and the linkage selected "average" [13].

Prediction of target genes

The following common softwares were used for prediction of the target genes, and the result was obtained from the intersection [14-16]. PicTar 2005: http://pictar.mdc-berlin.de/cgi-bin/PicTar_vertebrate.cgi; miRanda V5: http://www.ebi.ac.uk/enright-srv/microcosm/htdocs/targets/v5/; TargetScan 5.1: http://www.targetscan.org/.

Gene ontology (GO) analysis of target genes

The GO database included three aspects of function information regarding the biological process with gene involvement, the position in cells and the molecular function, and the function concepts were organized to the directed acyclic graph (DAG) structure. In the gene expression profiling, GO was usually used for providing the background knowledge regarding gene function classification tags and gene function study. The two target gene clusters with up- and down-regulated expression were projected into various nodes in the GO database, and the gene number in each node was calculated. The GSEABase soft package in the R statistical program (http://www.r-project.org/) was used.

Pathway analysis of target genes

The target genes were projected into the KEGG pathway database using the software GenMAPP version 2.1, and the enrichment P-values of genes were calculated in each pathway.

Analysis of transcription factor binding sites

The 2500 bp upstream and 500 bp downstream of the transcriptional initiation site of all differentially expressed miRNAs were extract-

Table 1. Growth and metastasis of the transplanted primary H460-GFP cells at different time after injection

Day after transplantation (d)	No. of nude mice sacrificed	No. of nude mice with natural death	Volume of primary tumor (Mean ± SD, mm^3)	No. of mice with mediastinal lymph node metastasis	No. of mice with right hilar lymph node metastasis	No. of mice with right lung metastasis	No. of mice with transverse septum metastasis	No. of mice with pericardial metastases	Total metastatic rate (%)*
15	8	0	218.9 ± 24.7	2	1	0	0	0	3/8
23	4	0	677.4 ± 22.3	2	0	0	0	0	2/4
30	8	2	921.1 ± 37.8	6	3	2	1	1	6/10
37	14	2	1335.7 ± 38.4	11	5	2	1	0	11/16
45	2	1	2867.5 ± 34.9	2	1	1	0	0	3/3

*Total metastatic rate (%) = No. of nude mice with metastases/No. of nude mice dissected × 100%.

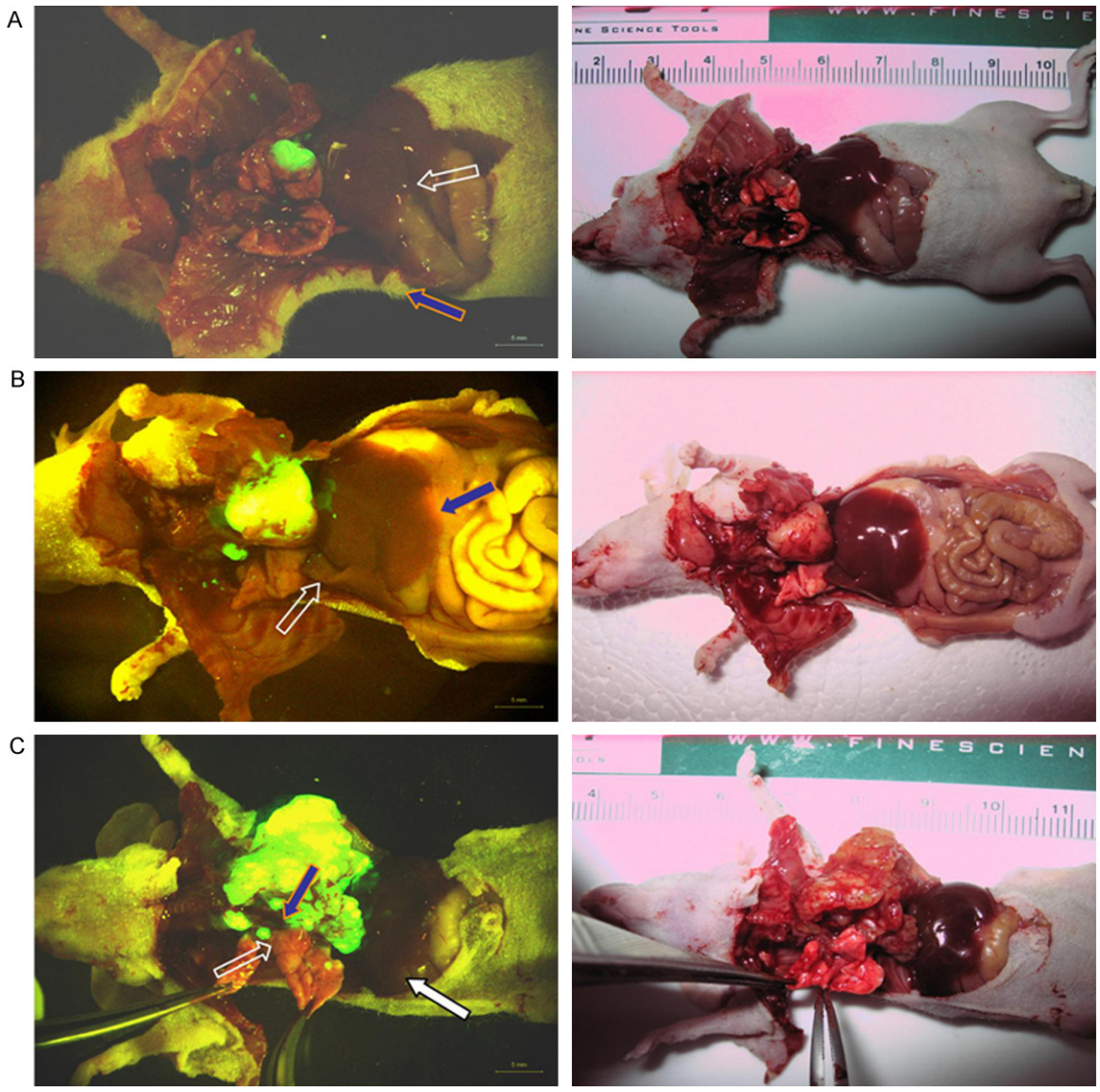

Figure 1. Nude mice with single or multiple metastatic foci under fluorescence stereo microscope and gross picture. A. The picture of nude mice without metastasis. The white hollow arrow shows the primary tumor on left lung, the blue solid indicates the normal right lung. B. The picture of nude mice with single metastatic foci. The yellow solid arrow shows the primary tumor on left lung, the white hollow arrow indicates the mediastinal lymph node metastatic foci. C. The picture of nude mice with multiple metastatic foci. The white hollow arrow shows the mediastinal lymph node metastatic foci, the blue solid arrow indicates the right hilar lymph node metastatic foci, and the white solid arrow indicates the metastatic foci on right lung.

ed. The transcription factor database TRANSFAC 7.0 public was used for analysis of initiator sequences. The transcription factor binding sites were predicted using the program patser (http://ural.wustl.edu/resources.html), and the relative score was set as > 0.9.

Regulatory network analysis

By integrating the regulation between miRNAs and target genes, and the mediation of miRNAs by transcription factors, the regulatory network among miRNAs, target genes and transcription factors was generated using the software Cytoscape (http://www.cytoscape.org/).

Real-time quantitative RT-PCR validation

According to the differentially expressed miRNAs with ratios between groups > 1.5 times or < 0.65 times screened by microarrays, in combination with the NSCLC metastasis regulation-

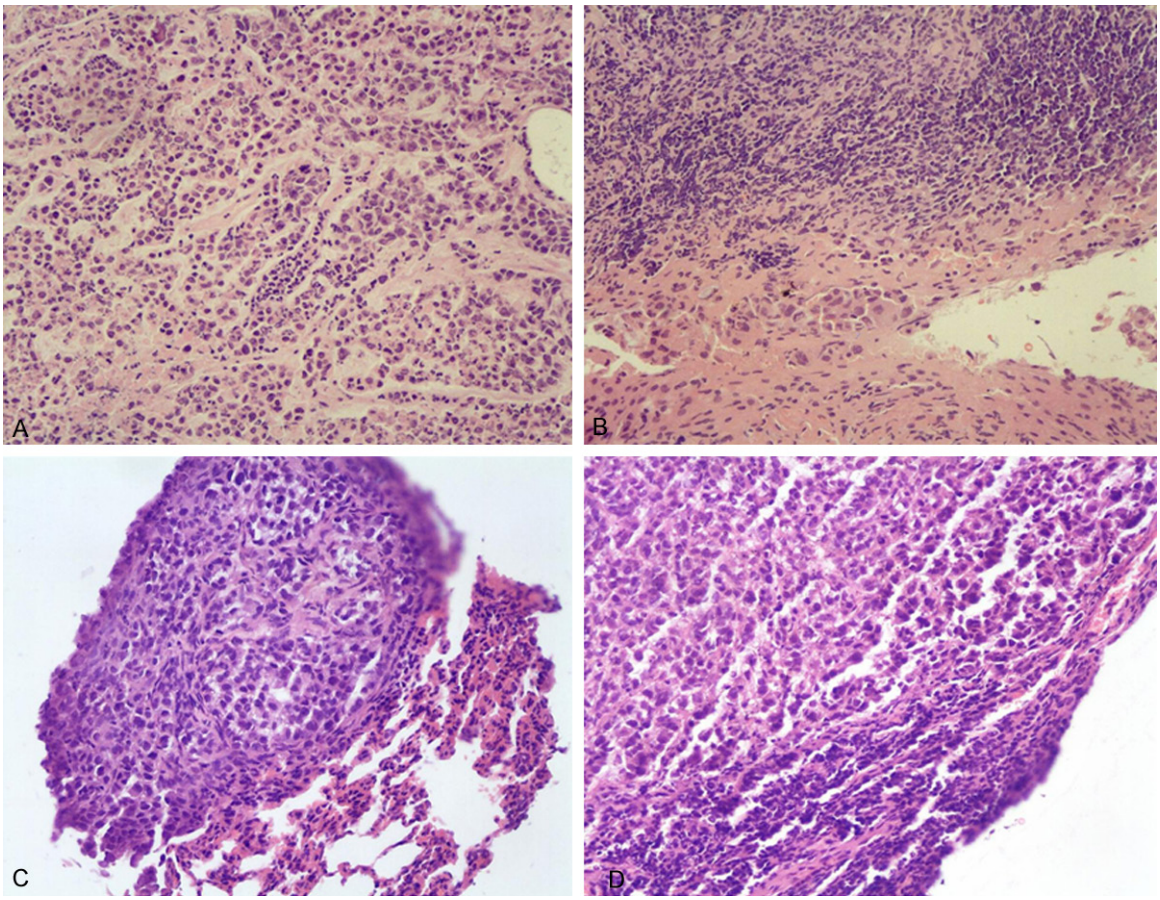

Figure 2. HE staining for the mediastinal lymph node metastatic foci under a microscope. A. HE staining of sections of the primary foci on the left lung (×200). B. HE staining of sections of the mediastinal lymph node metastatic foci (×200). C. HE staining of sections of the metastatic foci on the right lung (×200). D. HE staining of sections of the right hilar lymph node metastatic tumor (×200).

related target genes and miRNAs revealed by bioinformatics analysis, some miRNAs were selected for real-time quantitative RT-PCR validation. RNA was extracted using the Trizol reagent kit, and reverse transcription reaction was performed for synthesis of cDNA on a PCR amplifier. Relative quantitative PCR detection was performed using the Sybergreen (Invitrogen) dye method on the ABI Prism 7900 Sequence Detection System. U6 was used as internal reference, each reaction was repeated 3 times, and the cycle threshold (Ct value) was expressed by the mean value. The PCR reaction condition was at 95°C for 5 min, with 40 cycles. Data were analyzed using the $2^{-\Delta\Delta Ct}$ method.

Statistical analysis

The volumes of primary transplanted tumors were calculated in **Table 1**. All data were expressed as mean ± standard deviation (SD), and all statistical analyses were performed using the statistical software SPSS version 13.0. The data analyses and statistical analyses of miRNA microarray detection, bioinformatics analysis and real-time quantitative RT-PCR validation were described as above mentioned.

Results

Fluorescent transfection of H460 cells

After 24-72 h of transfection, the H460-GFP lung cancer cells obtained by the PT67-pLPCX-GFP-transfected H460 cells emitted strong green fluorescence under blue light, and the positive rate of GFP expression was about 90% (Data not shown).

Growth and metastasis following orthotopic implantation on nude mice

Natural death was observed in 5 out of 46 nude mice prior to the sacrifice, and metastases

Table 2. miRNAs expression determined using miRNA microarray

microRNA name	Ratio in Group A	*P* value	Regulation
hsa-miR-9	0.513703	0.002219	Down-regulation
hsa-miR-487b	0.519319	0.001241	Down-regulation
hsa-miR-302e	0.539167	0.004202	Down-regulation
hsa-miR-197	0.583689	0.005646	Down-regulation
hsa-miR-34b	0.594804	0.010702	Down-regulation
hsa-miR-31	0.619606	0.000190	Down-regulation
hsa-miR-374a	0.633897	0.045309	Down-regulation
hsa-miR-140-3p	1.551432	0.049092	Up-regulation
hsa-miR-129-5p	1.552450	0.010142	Up-regulation
hsa-miR-483-5p	1.574305	0.042309	Up-regulation
hsa-miR-296-5p	1.631601	0.025065	Up-regulation
hsa-miR-489	1.735225	0.026254	Up-regulation
hsa-miR-299-5p	1.853741	0.020911	Up-regulation
hsa-miR-127-5p	1.904299	0.009323	Up-regulation
hsa-miR-378	2.041047	0.044381	Up-regulation
hsa-miR-136	2.076979	0.029656	Up-regulation
hsa-miR-490-5p	2.366702	0.00188	Up-regulation
hsa-miR-208a	2.377387	0.008612	Up-regulation
hsa-miR-202	2.704407	0.017291	Up-regulation
hsa-miR-379	2.855973	0.032209	Up-regulation
hsa-miR-144	2.891786	0.038692	Up-regulation
hsa-miR-10b	3.215242	0.019688	Up-regulation
hsa-miR-205	3.299635	0.007460	Up-regulation
hsa-miR-451	3.391433	0.027467	Up-regulation
microRNA name	Ratio in Group B	*P* value	Regulation
hsa-miR-202	0.219985	0.000215	Down-regulation
hsa-miR-296-5p	0.347058	0.000084	Down-regulation
hsa-miR-92a	0.359559	0.006977	Down-regulation
hsa-miR-326	0.373480	0.011006	Down-regulation
hsa-miR-198	0.433532	0.007426	Down-regulation
hsa-miR-489	0.459701	0.010411	Down-regulation
hsa-miR-423-5p	0.496108	0.001277	Down-regulation
hsa-miR-147b	0.498099	0.042430	Down-regulation
hsa-miR-423-3p	0.505681	0.001232	Down-regulation
hsa-miR-129-5p	0.515690	0.000107	Down-regulation
hsa-miR-483-5p	0.558565	0.018858	Down-regulation
hsa-miR-339-3p	0.565076	0.014175	Down-regulation
hsa-miR-92b	0.569215	0.030819	Down-regulation
hsa-miR-484	0.595075	0.023668	Down-regulation
hsa-miR-25	0.635789	0.017739	Down-regulation
hsa-miR-492	0.644407	0.020063	Down-regulation
hsa-let-7g	1.500944	0.002003	Up-regulation
hsa-miR-34b	1.528312	0.022985	Up-regulation
hsa-miR-494	1.535862	0.002241	Up-regulation
hsa-miR-30e	1.610943	0.041878	Up-regulation
hsa-miR-497	1.644439	0.008635	Up-regulation
hsa-let-7e	1.655107	0.005946	Up-regulation

were detected in all 5 mice by postmortem examination. Fluorescence imaging revealed local metastases in 3 nude mice, however, the pathological examinations of tissues in the corresponding sites showed no metastasis. Postmortem examination indicated free implantation in thoracic cavity of 2 nude mice; the mice with metastasis in upper organs of thoracic cavity were excluded. No metastases were detected in 16 nude mice by postmortem examination, and the left 20 nude mice had metastases on different organs indicated by postmortem examination, and their tissue specimens were collected. The nude mice with metastasis included multiple metastases, and all nude mice with metastases had mediastinal lymph node metastases (**Table 1**).

Anatomy of animal models

The anatomical figures of animal models were shown in **Figure 1**.

Pathological examination

The pathological examinations of all 46 GFP-positive primary loci tissue specimens revealed low-differentiation carcinoma. Except that GFP was positive while pathological examination detected no infiltration of tumor cells in the mediastinal lymph node of a case, right hilar lymph node of a case and pericardial tissues of a case, the pathological examinations of the GFP-positive metastatic loci tissue specimens all revealed metastases (**Figure 2**). The coincidence rate between the fluorescence imaging and pathological examination was 92.3%.

miRNA microarray analysis

In comparison to the primary lesions on the left lung of nude mice without metastases (Group A), there were 17 miRNAs with up-regulated expression and 7 miRNAs with down-regulated expression on the primary foci

hsa-miR-337-3p	1.684633	0.003579	Up-regulation
hsa-miR-338-5p	1.729264	0.016106	Up-regulation
hsa-miR-146b-5p	1.736796	0.031588	Up-regulation
hsa-miR-486-5p	1.893567	0.014392	Up-regulation
hsa-miR-490-3p	1.964172	0.001443	Up-regulation
hsa-miR-340	2.067369	0.001391	Up-regulation
hsa-miR-495	2.103060	0.011562	Up-regulation
hsa-miR-212	2.274477	0.012768	Up-regulation
hsa-miR-302e	2.291677	0.001529	Up-regulation
hsa-miR-146b-3p	2.304957	0.003745	Up-regulation
hsa-miR-422a	2.984432	0.048098	Up-regulation
hsa-miR-297	2.984726	0.000832	Up-regulation
hsa-miR-302f	3.369296	0.028652	Up-regulation
hsa-miR-491-3p	4.137266	0.000168	Up-regulation

of the left lung of nude mice with metastases. Compared with the primary lesions on the left lung of nude mice with metastases (Group B), there were 20 miRNAs with up-regulated expression and 16 miRNAs with down-regulated expression on the metastatic foci on the nude mice with metastases (**Table 2**).

Bioinformatics analysis

Hierarchical clustering analyses were performed in all differentially expressed miRNAs (**Figure 3**). The color indicated the intensity of signal value, the signal value increased sequentially from green, black, to red. A total of 128 genes were predicted in the intersection by the 3 softwares TargetScan + miRanda + PicTar in Group A, and these genes had a high possibility of being the real target genes. For example, it was highly possible that *RARβ* and *E2F-1* played key roles in the initial mechanisms of NSCLC metastasis. In Group B, 63 genes were identified in the intersection predicted by the 3 softwares, and the genes like *RASSF1*, *E2F-3* and *TCF7L1* were highly possible to play critical roles in the mediation mechanisms of metastasis development (**Figure 4**). The differentially expressed genes were classified according to the 3 independent manners of biological process, cellular component and molecular function (**Figure 5**).

Pathway analysis detected 62 pathways in Group A, including 22 pathways with gene count ≥ 2, and retinoic acid receptor β (*PARβ*) and *E2F1* were the target genes up-regulating miR-144 and miR-205, respectively in NSCLC-related signal pathway (**Figure 6A**). Pathway analysis observed 47 pathways in Group B, including 10 pathways with gene count ≥ 2, and *RASSF1* and *E2F3* were the target genes down-regulating miR-326 and miR-25, respectively in NSCLC-related signal pathway (**Figure 6B**). Analysis of transcription factor binding sites demonstrated that, the transcription factors like activator protein 1 (AP-1), p53, CEBPB, NF-κB, c-Myc and E2F may mediate the differentially expressed miRNAs in Group A, while the transcription factors like AP-1, AP-4, p53, NF-κB, E2F and SP-1 may mediate the differentially expressed miRNAs in Group B (**Figure 7**).

In the regulatory network map, the solid edge indicated the regulation of target genes by miRNAs, the dotted edge indicated the regulation of related miRNAs by transcription factors; while red nodes indicated miRNAs, green nodes indicated transcription factors and grey nodes indicated target genes (**Figure 8**).

Real-time quantitative RT-PCR analysis

A total of 24 differentially expressed miRNAs were identified in Group A, while 36 were detected in Group B (**Figure 1**). The NSCLC-associated Pathway analysis revealed miR-144 and miR-205 in Group A and miR-25 and miR-326 in Group B and their corresponding target genes were possible to be involved in metastasis occurrence and development (**Figure 6**). The regulatory network demonstated that miR-10b, miR-34b, miR-144, miR-31, miR-9 from Group A and miR-25, miR-326, miR-202 and miR-92a from Group B were highly correlated with the metastasis-related target genes and transcription factors (**Figure 8**). Based on aforementioned results, combined with previous studies, miR-let-7 [17, 18] and miR-205 [19, 20] were involved in mediation of metastasis of many malignant tumors including NSCLC. Therefore, 6 miRNAs in Group A including miR-10b, miR-34b, miR-144, miR-31, miR-9 and miR-205, and 5 miRNAs in Group B including miR-25, miR-326, miR-202, miR-92a and miR-let-7e were selected for further real-time quantitative RT-PCR validation.

The corresponding tissue specimens from 16 nude mice without metastases and 20 nude mice with metastases were used from RT-PCR

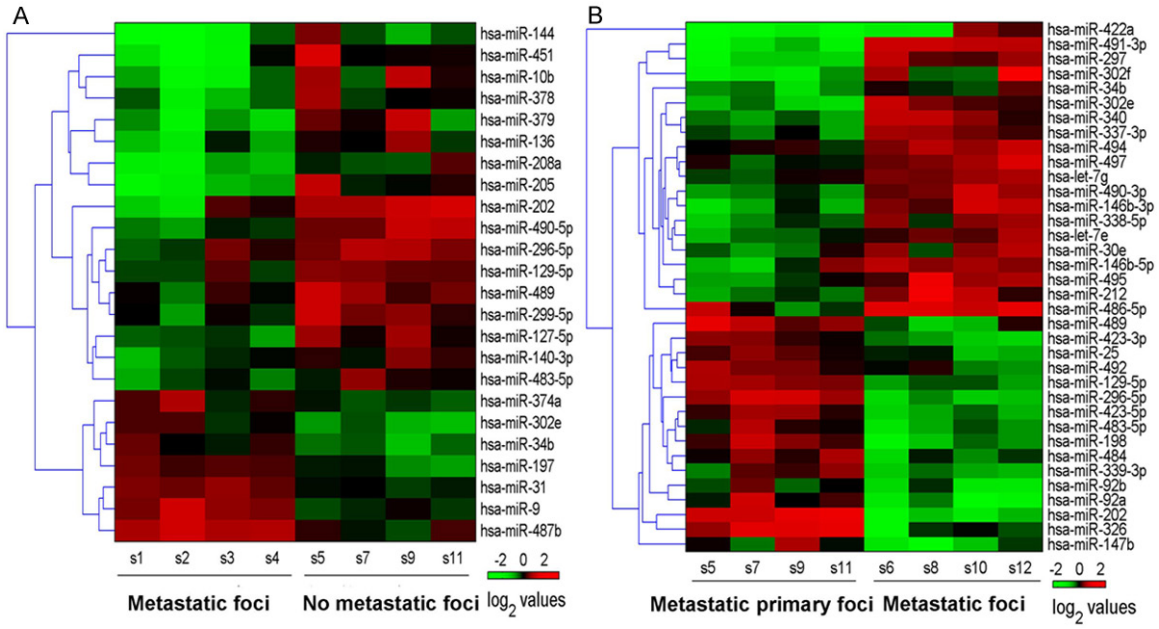

Figure 3. Hierarchical clustering map of the differentially expressed miRNAs in Group A (A) and Group B (B).

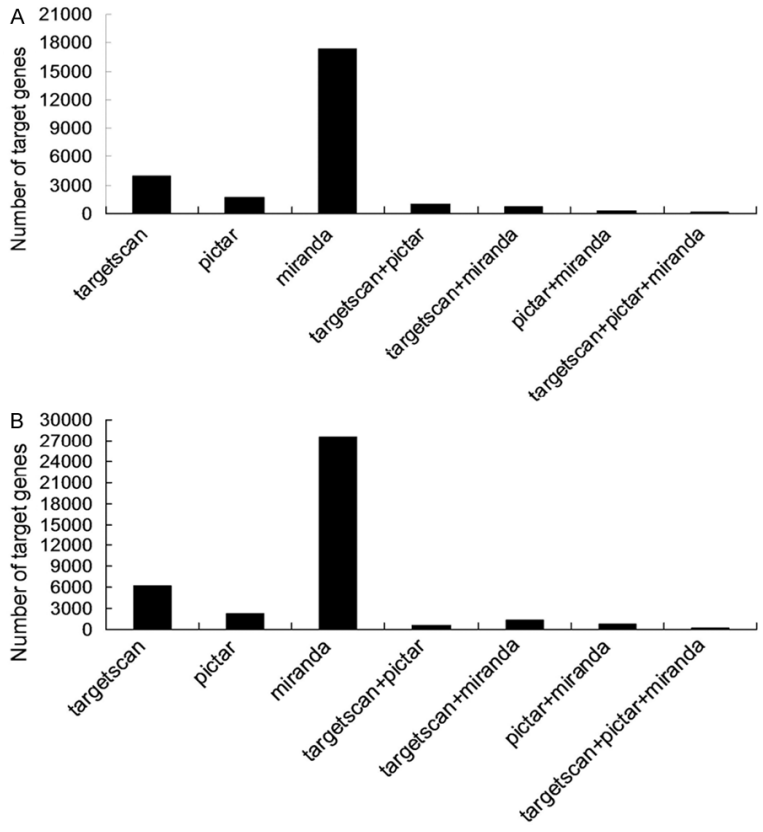

Figure 4. Prediction of target genes of the differentially expressed miRNAs in Group A (A) and Group B (B). Longitudinal axis is the number of target genes, horizontal axis is the prediction software used.

validation. The primers for RT-PCR analysis were designed using the software Primer 5.0, and synthesized by the Shanghai Invitrogen Bio-tech Co., Ltd (Shanghai, China), and the sequences of primers were listed in **Table 3**.

The data from the real-time quantitative RT-PCR were analyzed using the $2^{-\Delta\Delta Ct}$ method, and figures were generated based on the difference of gene expression among specimens (vertical coordinate) and the corresponding miRNAs (horizontal coordinate) (**Figure 9**). Figures were plotted based on the difference folds of miRNAs ratio (ratio > 1 was defined as up-regulation, ratio < 1 was defined as down-regulation) (vertical coordinate), and the corresponding miRNAs (horizontal coordinate). miRNA microarray analysis revealed consistent regulation in 6 miRNAs from Group A; in Group B, except that miR-let-7e expression was up-regulated in miRNA microarray but down-regulated in RTPCR, consistent regulation was observed in other 4 miRNAs (**Figure 10**).

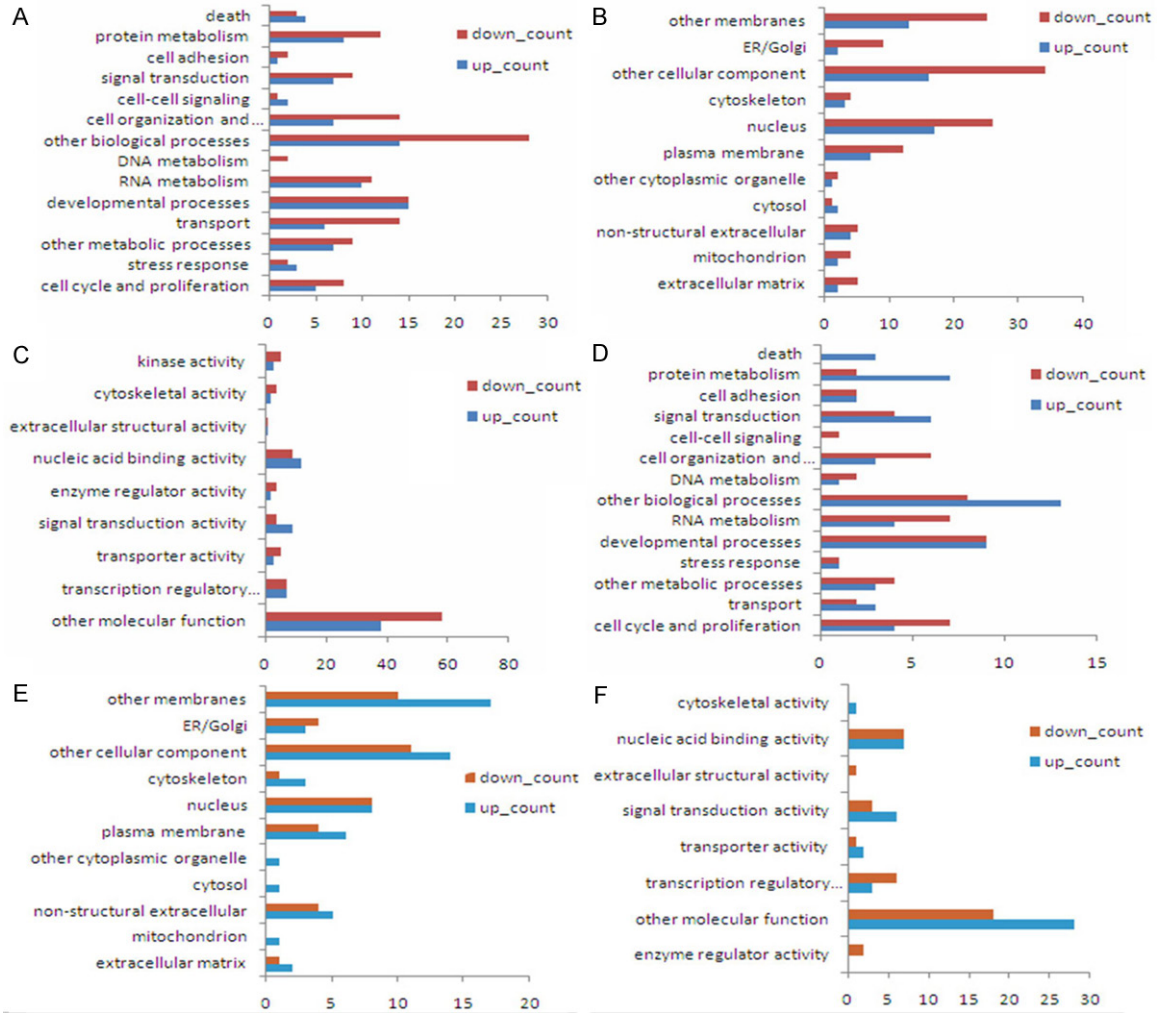

Figure 5. The biological process classification (A, D) cellular component classification (B, E) and molecular function classification (C, F) of target genes in groups A and B. Longitudinal axis is the category of gene functions, horizontal axis is the proportions of the number of target genes with this function in total number of target genes.

Discussion

Currently, GFP is one of the best *in-vivo* molecular markers, which is widely applied in studies at cellular and sub-cellular levels, notably in determination of the tumor volume and infiltration range. The present study used the GFP-transfected human large cell lung cancer cell line H460 to establish orthotopic implantation animal models of lung cancer, and carried out real-time and non-invasive observation on tumor growth in nude mice using the fluorescence stereo microscope, so as to accurately determine the tumor size and metastatic organs.

It has been demonstrated that miRNAs mediate the metastatic process of multiple malignant tumors. Ma et al. [21] observed miR-10b was involved in breast cancer invasion and metastasis. In colorectal and breast cancer cell lines with high metastatic characteristics, miR-21 functions through regulation of the tumor suppressor genes like *PTEN*, *PDCD4* and *TPM1* [9, 22, 23], and high expression of miR-21 is correlated with advanced staging of breast cancer and lymph node metastasis [24]. Up-regulation of miR-373 and miR-520c inhibits CD44 expression, and thus promotes tumor invasion and metastasis [25]. miR-155 leads to increase in invasion of mammary epithelial cells through regulation of target gene *RhoA* [26]. Gregory et al. [18, 27] reported that miR-200 family and miR-205 led to epithelial to mesenchymal transition (EMT), which was considered as an essential step in early tumor

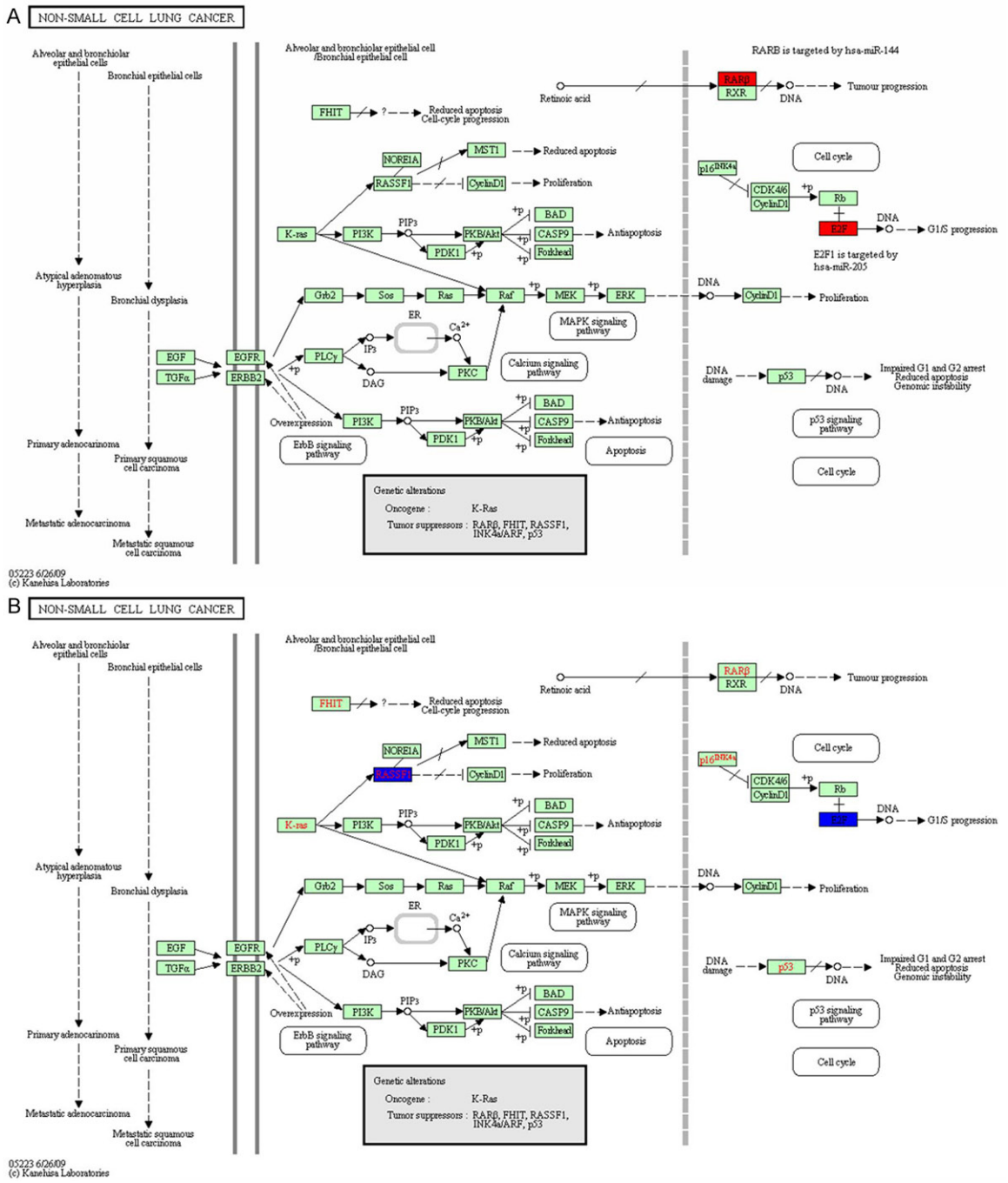

Figure 6. Pathway analysis in groups A (A) and B (B).

metastasis. Lujambio and colleagues [28] observed silencing of miRNAs with tumor suppressor features by DNA methylation caused tumor metastasis. It has been reported that miR-10b, miR-9, miR-31, miR-34b, miR-92a, miR-205 and miR-202 mediate metastases of malignant tumor like lung cancer, breast cancer, ovarian cancer, gastric cancer, prostate cancer and bladder cancer mainly through the mechanisms such as DNA methylation in the promoter region, EMT and signal transduction pathway. However, there are few studies reporting the roles of miR-25, miR-144 and miR-326 in tumor metastasis.

The target genes of the differentially expressed miRNAs were mainly involved in regulation of cell proliferation, cell cycle and development,

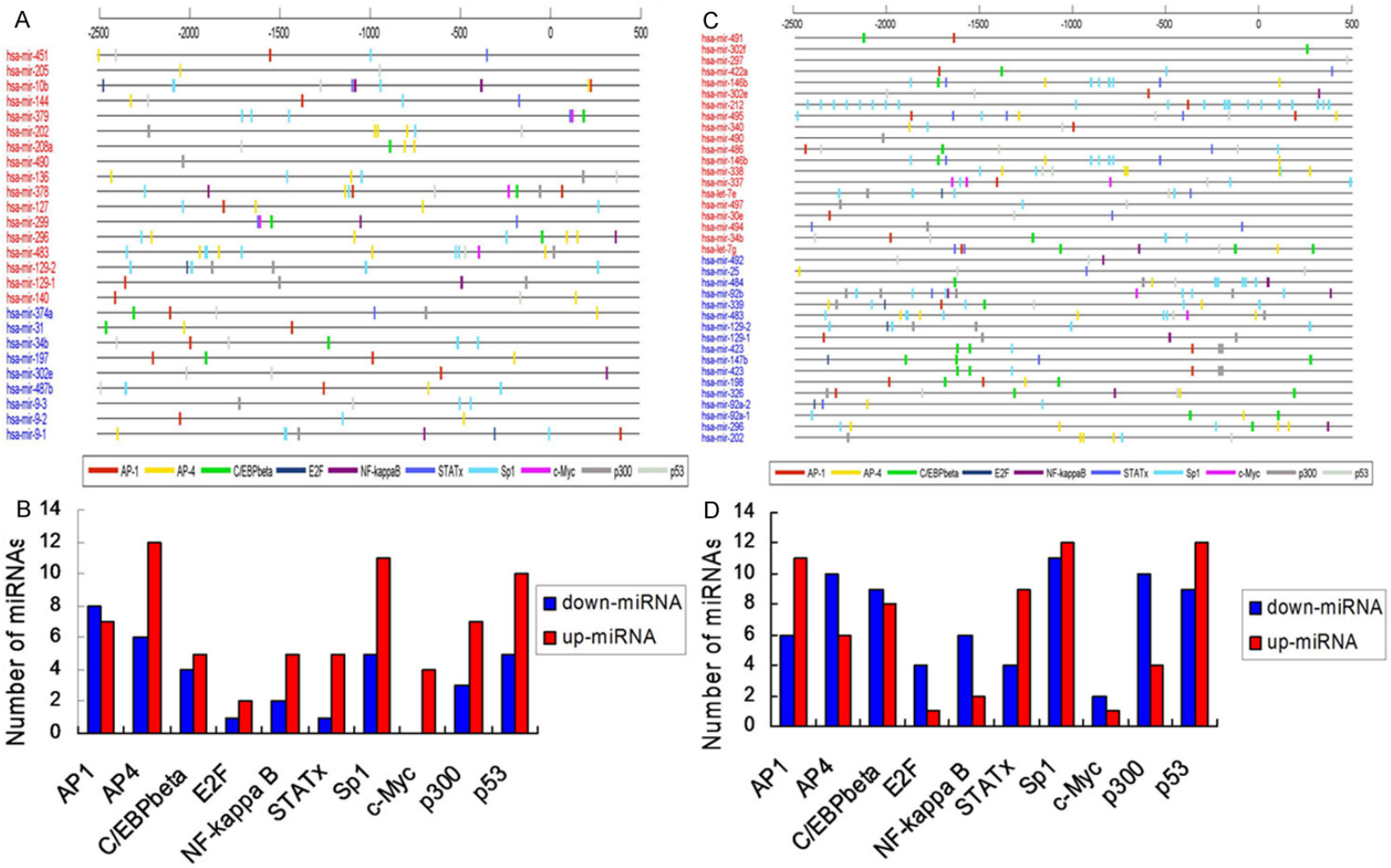

Figure 7. Analysis of transcription factor loci (A, C) and distribution of related transcription factors (B, D) in groups A and B. In **Figure 8B** and **8D**, longitudinal axis is the number of miRNAs regulated by transcription factors, horizontal axis is the name of the corresponding transcription factors.

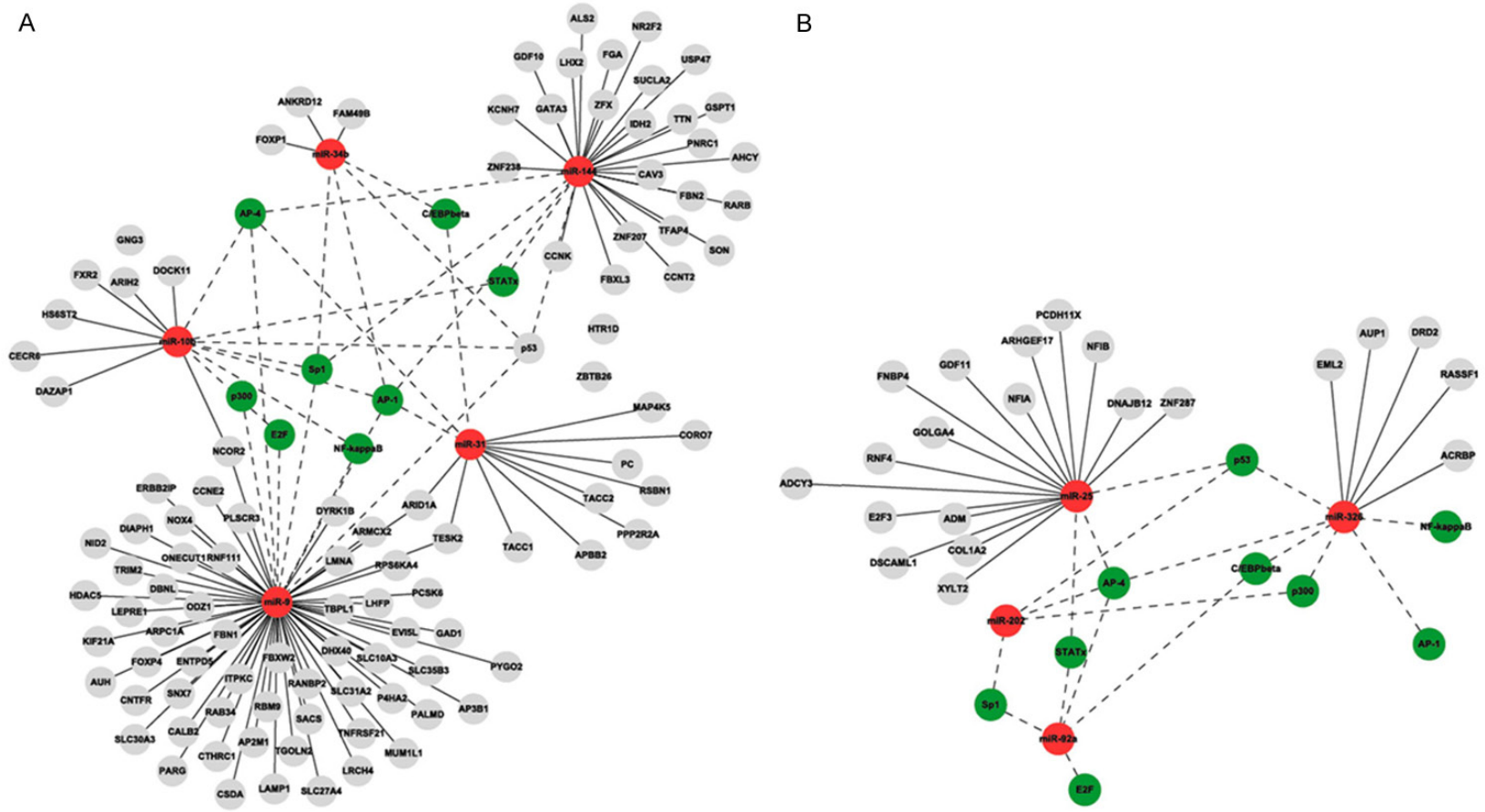

Figure 8. miRNAs regulation network in groups A (A) and B (B).

Table 3. Primers for real-time quantitative PCR

Gene name	Sequence of double-strand primers*
U6	F: 5'-TGGGGTTATACATTGTGAGAGGA-3',
	R: 5'-GTGTGCTACGGAGTTCAGAGGTT-3'.
hsa-miR-10b	F: 5'-GGATACCCTGTAGAACCGAA-3',
	R: 5'-CAGTGCGTGTCGTGGAGT-3'.
hsa-miR-31	F: 5'-GGAGGCAAGATGCTGGC-3',
	R: 5'-CAGTGCGTGTCGTGGAGT-3'.
hsa-miR-205	F: 5'-GCTCCTTCATTCCACCG-3',
	R: 5'-CAGTGCGTGTCGTGGAGT-3'.
hsa-miR-144	F: 5'-GGGGGTACAGTATAGATGAT-3',
	R: 5'-TGCGTGTCGTGGAGTC-3'.
hsa-miR-9	F: 5'-GGGTCTTTGGTTATCTAGC-3',
	R: 5'-TGCGTGTCGTGGAGTC-3'.
hsa-miR-202	F: 5'-GGGGAGAGGTATAGGGCA-3',
	R: 5'-CAGTGCGTGTCGTGGAGT-3'.
hsa-let-7e	F: 5'-CAGTGCGTGTCGTGGAGT-3',
	R: 5'-CGGTGAGGTAGGAGGTTGTAT-3'.
hsa-miR-34b	F: 5'-TGCGTGTCGTGGAGTC-3',
	R: 5'-GCGAATCACTAACTCCACT-3'.
hsa-miR-25	F: 5'-CCAGTGCGTGTCGTGGA-3',
	R: 5'-GGCATTGCACTTGTCTCG-3'.
hsa-miR-326	F: 5'-CCAGTGCGTGTCGTGG-3',
	R: 5'-CCTCTGGGCCCTTCCT-3'.
hsa-miR-92a	F: 5'-ATCCAGTGCGTGTCGTG-3',
	R: 5'-GGTATTGCACTTGTCCCG-3'.

*F (Forward) is the corresponding miRNAs specific primer, R (Reverse) is the primer matched with RT-PCR primers.

DNA and/or RNA metabolism, and signal transduction pathway. Bioinformatics analysis of miRNAs and Pathway analysis (**Figure 6A**) and regulatory network analysis of target genes (**Figure 8A**) all indicated the target gene that up-regulated miR-144 expression may be PARβ, which bound with all-trans retinoic acid (ATRA) to mediate the effect of retinoic acid. Up-regulation of miR-144 inhibits the role of PARβ in blocking tumor cell metastasis, which is characterized in the following aspects. Angiogenesis is particularly important during the process of malignant tumor metastasis, and the new angiogenesis of tumor tissues is positively proportional to invasion and metastasis of cancer tissues. It has been shown that ATRA down-regulates tumor growth factor-beta (TGF-β) expression, and significantly inhibits the proliferation of vascular smooth muscle cells [29]. In addition, ATRA significantly reduces the synthesis of low collagen, fibronectin and laminin, leading to reduction of motility in tumor cells [30]. Immunosuppression caused by tumor is another important mechanism for escaping from immunological surveillance and the resultant invasion and infiltration. ATRA increases the killing ability of natural killer (NK) cells and lymphokine-activated killer (LAK) cells through inducing the differentiation of the immature bone marrow cells, improves tumor-specific immune response mediated by $CD4^+$ and $CD8^+$ cells, up-regulates the expression of RARα and RARβ in blood lymphocytes, promotes the expression of cytokines which play important roles in immune process and destroys the tumor cells in the circulatory system and the emerged minor metastatic lesions, leading to inhibition of occurrence and development of tumor metastasis [30, 31]. The Pathway (**Figure 6B**) and regulatory network analyses (**Figure 8B**) of miRNAs and target genes all revealed the target gene which up-regulated miR-326 expression may be Ras association domain-containing protein family 1 (RASSF1), which is a novel tumor suppressor gene cloned from the small arm of human chromosome 3 [32]. Down-regulation of miR-326 inhibits the anti-tumor and anti-metastatic activity of RASSF1. In primary lung cancer and breast cancer, hypermethylation of RASSF1A in the promoter 5' CpG island region is closely related with the pathological progression of the disease. More distinct tumor local invasion, more distant lymph node metastasis and more advanced tumor stage lead to higher incidence of methylation [33]. The mechanism may be the imbalance of RAS caused by inhibition of RASSF1, or the blockage of accumulation of cyclin D1 and shift from G1 phase to S phase in the cell cycle [34, 35], leading to promotion of malignant tumor formation and metastasis. It is predicted that *E2F-1* is the target gene to up-regulate miR-205 expression, and *E2F-3* is the target gene to down-regulate miR-25 expression, both belonging to nuclear transcription factor E2F family. E2F is the most important transcription factor in the Rb/E2F pathway, which exhibits dual regulatory effect on cell transcription, proliferation and apoptosis, and whether it acts as oncogene or tumor suppressor gene is determined by the degree of the dual effect and is associated with organ-specificity. Lujambio et al. [28] reported that the reduction in expression of oncogenes like *E2F-3* and *C-myc* inhibited tumor metastasis. High expression of *E2F-1* in head and neck can-

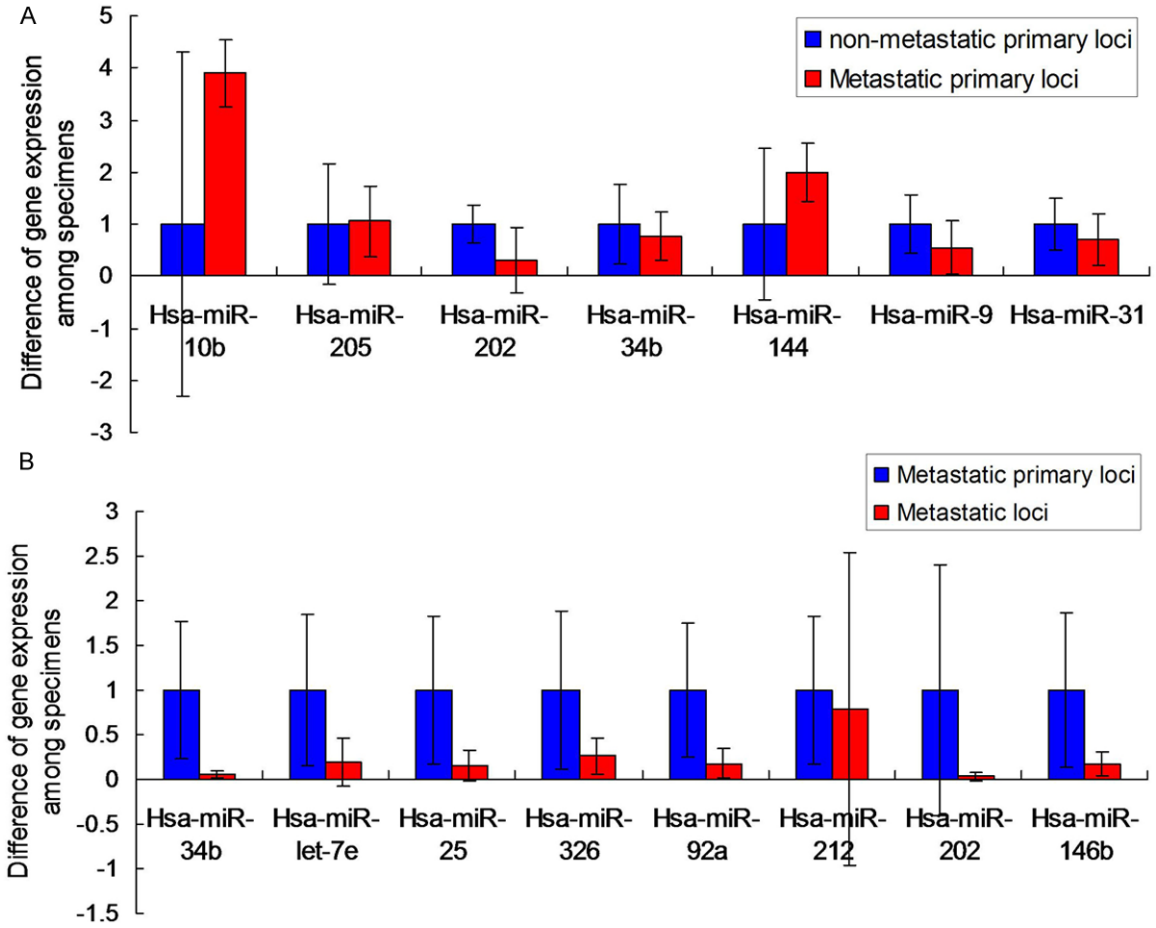

Figure 9. RT-PCR validation of samples from groups A (metastatic primary loci vs. non-metastatic primary loci) (A) and B (metastatic loci vs. metastatic primary loci) (B).

cer is closely related with tumor metastasis and prognosis [36].

GO analysis and transcription factor binding site analysis of target genes demonstrated that it was highly possible the transcription factors AP-1, AP-4, p53, STATs and NF-κB were involved in regulation of NSCLC metastasis-related miRNAs. AP-1 inhibits cell growth through regulation of cell cycle regulators cyclin D, cyclin A, p53, p21Cip, p16INK4a and p19Arf [37]. Many target gene products mediated by AP-1 are involved in the invasion and metastasis of tumor cells, which needs degradation of extracellular matrix components to enable angiogenesis and cell migration. In addition, AP-1 mediates the transcription of tumor metastasis-related factors like CD44, cathepsin L and MTS1. p53 is a protein referring to cell cycle regulation and apoptosis, its wild type acts as a tumor suppressor gene, while the mutant type functions as an oncogene. It is considered that the mutant p53 protein enables cell survival under anoxic conditions, and promotes angiogenesis and metastasis of tumors through inducing the expression of inducible NO synthase (iNOS) and vascular endothelial growth factor (VEGF) [38]. Signal transducer and activator of transcription (STAT) is an important member in the JAKs-STATs transduction pathway. The STATs family, notably STAT3, plays important roles in promoting tumor cell proliferation, inhibiting tumor cell apoptosis and promoting invasion and metastasis, as well as immune evasion. STAT3 regulates cell growth, differentiation and apoptosis through mediating the transcription of the downstream target genes, notably cyclin D1. In addition, activation of NF-κB up-regulates the expression of VEGF, E-selectin, integrin, ICAM-1, VCAM-1 and MMP-9 which are associated with tumor metastasis, and chemical factor receptors like CXCR4, uPA and IL-8, through increasing the adhesion ability of tumor cells, degrading surrounding

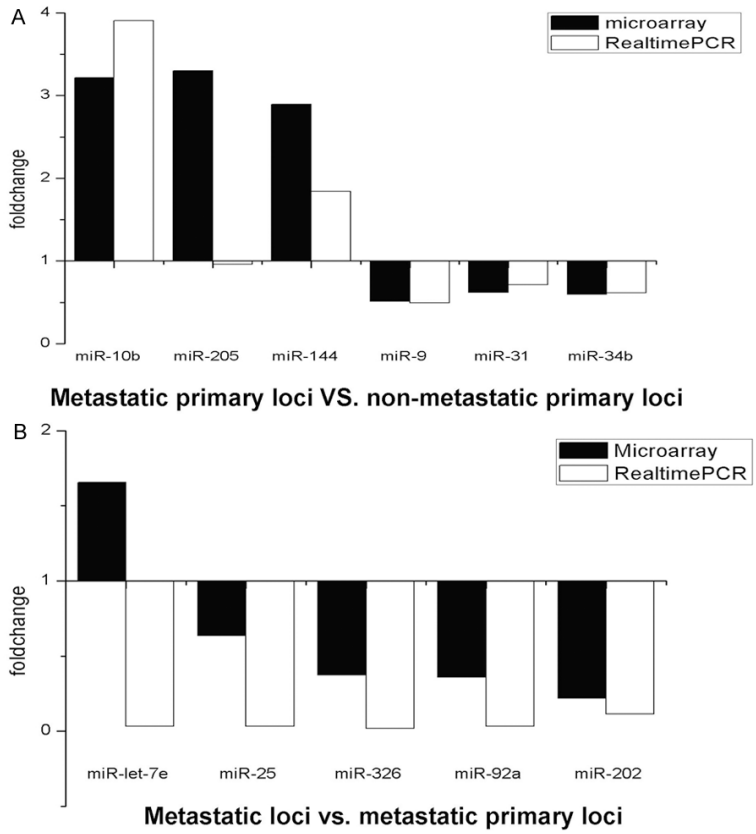

Figure 10. Comparison of miRNAs microarray and RT-PCR analysis of differentially expressed miRNAs in groups A (A) and B (B).

matrix, promoting EMT and tumor angiogenesis [39-41]. Therefore, most of these transcription factors are involved in the proliferation, differentiation, transformation and apoptosis, as well as regulation of cell cycle signal pathway.

Comparison between miRNA microarray and RT-PCR validation showed that there was big difference of difference fold value of miR-205 expression between the miRNA microarray and RT-PCR analysis (**Figure 10A**) in Group A. miRNA microarray analysis revealed that miR-let-7e was up-regulated, while it was down-regulated in RT-PCR validation in Group B (**Figure 10B**), which may attribute to the variation in sample size used in miRNA microarray and RT-PCR. In the present study, miRNA microarray used 4 pairs of nude mice with and without metastases, while 16 nude mice without metastases and 20 mice with metastases were used in RT-PCR. Due to small sample size, miRNA microarray is only used as a tool for preliminary screening, and the probability of "false positive" and/or "false negative" is relatively high. Therefore, the RT-PCR validation is more credible than the results revealed by the miRNA microarray.

The present study compared the difference of miRNA expression profiling in NSCLC tissues with and without metastases, and predicted the corresponding target genes and transcription factors of these differentially expressed miRNAs using bioinformatics method. The results showed that the differentially expressed miRNAs and the related target genes and transcription factors may be involved in the occurrence and development of NSCLC metastasis. Further studies to investigate the possibility that the expression profiling of these differentially expressed miRNAs is used as markers for detecting NSCLC metastasis and assessing prognosis seem justified. Curren-tly, the study to explore the role of miRNAs in NSCLC metastasis remains at a theoretical level, and the mechanism is still superficial. Therefore, further studies should be carried out to provide new ideas for exploring diagnosis, treatment and prognosis of tumor metastasis.

Acknowledgements

This work was funded by Jiangsu Provincial Special Program of Medical Science (BL2012-008).

Disclosure of conflict of interest

None to declare.

Address correspondence to: Yong-Qian Shu, Department of Oncology, The first affiliated Hospital of Nanjing Medical University, No. 300 Guangzhou Road, Nanjing 210029, JiangSu Province, China. E-mail: shu_yongqian@163.com

References

[1] Li B, Blanc JM, Sun Y, Yang L, Zaorsky NG, Giacalone NJ, Torossian A and Lu B. Assessment of M867, a selective caspase-3 inhibitor, in an

orthopic mouse model for non-small cell lung carcinoma. Am J Cancer Res 2014; 4: 161-171.
[2] Mountain CF and Dresler CM. Regional lymph node classification for lung cancer staging. Chest 1997; 111: 1718-1723.
[3] Ying H, Yang XD, Sun Z, Ning X, Wang Y, Bai C, Chen S and Wang Y. Lifestyle risks exposure and response predictor of gefitinib in patients with non-small cell lung cancer. Med Oncol 2014; 31: 220.
[4] Huang BW, Miyazawa M and Tsuji Y. Distinct regulatory mechanisms of the human ferritin gene by hypoxia and hypoxia mimetic cobalt chloride at the transcriptional and post-transcriptional levels. Cell Singnal 2014; 26: 2702-2709.
[5] Calin GA, Sevignani C, Dumitru CD, Hyslop T, Noch E, Yendamuri S, Shimizu M, Rattan S, Bullrich F, Negrini M and Croce CM. Human microRNA genes are frequently located at fragile sites and genomic regions involved in cancers. Proc Natl Acad Sci U S A 2004; 101: 2999-3004.
[6] Esquela-Kerscher A and Slack FJ. Oncomirs-microRNAs with a role in cancer. Nat Rev Cancer 2006; 6: 259-269.
[7] Rashidi B, Yang M, Jiang P, Baranov E, An Z, Wang X, Moossa AR and Hoffman RM. A highly metastatic Lewis lung carcinoma orthotopic green fluorescent protein model. Clin Exp Metastasis 2000; 18: 57-60.
[8] Salmon HW, Guha A, Rojiani AM and Siemann DW. Vascular development in mouse lung metastases. Am J Cancer Res 2012; 2: 581-588.
[9] Yang LX, Huang XF, Shao Q, Huang MY, Deng L, Wu QL, Zeng YX and Shao JY. MicroRNA miR-21 overexpression in human breast cancer is associated with advanced clinical stage, lymph node metastasis and patient poor prognosis. RNA 2008; 14: 2348-2360.
[10] Yang K, Li Z, Cao Y, Yu X and Mei J. Effect of peptide-conjugated near-infrared fluorescent quantum dots (NIRF-QDs) on the invasion and metastasis of human tongue squamous cell carcinoma cell line Tca8113 in vitro. Int J Mol Sci 2009; 10: 4418-4427.
[11] Huang P, McKee TD, Jain RK and Fukumura D. Green fluorescent protein (GFP)-expressing tumor model derived from a spontaneous osteosarcoma in a vascular endothelial growth factor (VEGF)-GFP transgenic mouse. Comp Med 2005; 55: 236-243.
[12] Liao W, Jordaan G, Srivastava MK, Dubinett S, Sharma S and Sharma S. Effect of epigenetic histone modifications on E-cadherin splicing and expression in lung cancer. Am J Cancer Res 2013; 3: 374-389.
[13] Zou Z, Hu C, Zhang F, Zhao H and Shen S. WSNs data acquisition by combining Hierarchical routing method and compressive sensing. Sensors (Basel) 2014; 14: 16766-16784.
[14] Muller S. In silico analysis of regulatory network underlines the role of miR-10b-5p and its target BDNF in huntington's disease. Transl Neurodegener 2014; 3: 17.
[15] An J, Lai J, Lehman ML and Nelson CC. miRDeep: an integrated application tool for miRNA identification from RNA sequencing data. Nucleic Acids Res 2013; 41: 727-737.
[16] Fujiwara S, Ida H, Yoshioka Y, Yoshida H and Yamaguchi M. The warts gene as a novel target of the Drosophila DRE/DREF transcription pathway. Am J Cancer Res 2012; 2: 36-44.
[17] Appari M, Babu KR, Kaczorowski A, Gross W and Herr I. Sulforaphane, quercetin and catechins complement each other in elimination of advanced pancreatic cancer by miR-let-7 induction and K-ras inhibition. Int J Oncol 2014; 1391-1400.
[18] Gregory PA, Bert AG, Paterson EL, Barrt SC, Tsykin A, Farshid G, Vadas MA, Khew-Goodall Y and Goodall GJ. The miR-200 family and miR-205 regulate epithelial to mesenchymal transition by targeting ZEB1 and SIP1. Nat Cell Biol 2008; 10: 593-601.
[19] Kim J, Lim NJ, Jang SG, Kim HK and Lee GK. miR-592 and miR-552 can distinguish between primary lung adenocarcinoma and colorectal cancer metastases in the lung. Anticancer Res 2014; 34: 2297-2302.
[20] Larzabal L, de Aberasturi AL, Redrado M, Rueda P, Rodriguez MJ, Bodegas ME, Montuenga LM and Calvo A. TMPRSS4 regulates levels of integrin alpha-5 in NSCLC through miR-205 activity to promote metastasis. Br J Cancer 2014; 110: 764-774.
[21] Ma L, Teruya-Feldstein J and Weinberg RA. Tumour invasion and metastasis initiated by microRNA-10b in breast cancer. Nature 2007; 449: 682-688.
[22] Asangani I, Rasheed SAK, Nikolova DA, Leupold JH, Colburn NH, Post S and Allgayer H. MicroRNA-21 post-transcriptionally downregulates tumor suppressor Pdcd4 and stimulates invasion,intravasion and metastasis in colorectal cancer. Oncogene 2008; 27: 2128-2136.
[23] Mishra S, Lin CL, Huang TH, Bouamar H and Sun LZ. MicroRNA-21 inhibits p57Kip2 expression in prostate cancer. Mol Cancer 2014; 13: 212.
[24] Walter BA, Gomez-Macias G, Valera VA, Sobel M and Merino MJ. miR-21 expression in pregnancy-associated breast cancer: a possible marker of poor prognosis. J Cancer 2011; 2: 67-75.
[25] Huang Q, Gumireddy K, Schrier M, Le Sage C, Nagel R, Nair S, Egan DA, Li A, Huang G, Klein-Szanto AJ, Gimotty PA, Katsaros D, Coukos G,

Zhagn L, Pure E and Agami R. The microRNAs miR-373 and miR-520c promote tumour invasion and metastasis. Nat Cell Biol 2008; 10: 202-210.

[26] Kong W, Yang H, He L, Zhao JJ, Coppola D, Dalton WS and Cheng JQ. MicroRNA-155 is regulated by the transforming growth factor beta/Smad pathway and contributes to epithelial cell plasticity by targeting RhoA. Mol Cell Biol 2008; 28: 6773-6784.

[27] Gregory PA, Bracken CP, Bert AG and Goodall GJ. MicroRNA as regulators of epithelial-mesenchymal transition. Cell Cycle 2008; 7: 3112-3118.

[28] Lujambio A, Calin GA, Villanueva A, Ropero S, Sanchez-Cespedes M, Blanco D, Montuenga LM, Rossi S, Nicoloso MS, Faller WJ, Gallagher WM, Eccles SA, Croce CM and Esteller M. A microRNA DNA methylation signature for human cancer metastasis. Proc Natl Acad Sci U S A 2008; 105: 13556-13561.

[29] Ostriker A, Horita HN, Pocazobutt J, Weiser-Evans MC and Nemenoff RA. Vascular smooth muscle cell-derived transforming growth factor-beta promotes maturation of activated, neointima lesion-like macrophages. Arterioscler Thromb Vasc Biol 2014; 34: 877-886.

[30] Wang W, Xu G, Ding CL, Zhao LJ, Zhao P, Ren H and Qi ZT. All-trans retinoic protects hepatocellular carcinoma cells against serum-starvation-induced cell death by upregulating collagen 8A2. FEBS J 2013; 280: 1308-1319.

[31] Liang QL, Chen GQ, Liu QL, Li ZY, Zhang XN, Zhou Y, Ou WT, Wang BR and Hu LR. Tumor suppressor TSLC1 inhibits growth, proliferation, invasiveness and angiogenesis in nude mice xenografted tumor of Eca109 cells. Int J Clin Exp Med 2014; 7: 1507-1515.

[32] Valencia K, Martin-Fernandez M, Zandueta C, ormazabal C, Martinez-Canarias S, Bandres E, de la Piedra C and Lecanda F. miR-326 associated with biochemical markers of bone turnover in lung cancer bone metastasis. Bone 2013; 52: 532-539.

[33] Dammann R, Schagdarsurengin U, Seidel C, Strunnikova M, Rastetter M, Baier K and Pfeifer GP. The tumor suppressor RASSF1A in human carcinogenesis: an update. Histol Histopathol 2005; 20: 645-663.

[34] Vos MD, Ellis CA, Bell A, Birrer MJ and Clark GJ. Ras uses the novel tumor supressor RASSF1 as an effector to mediate apoptosis. J Biol Chem 2000; 275: 35669-35672.

[35] Agathanggelou A, Honorio S, Macartney DP, Martinez A, Dallol A, Rader J, Fullwood P, Chauhan A, Walker R, Shaw JA, Hosoe S, Lerman MI, Minna JD, Maher ER and Latif F. Methylation associated inactivation of RASSF1A from region 3p21.3 in lung, breast and ovarian tumors. Oncogene 2001; 20: 1509-1518.

[36] Zhang SY, Liu SC, Johnson DG and Klein-Szanto AJ. E2F-1 gene transfer enhances invasiveness of human head and neck carcinoma cell lines. Cancer Res 2000; 60: 5972-5976.

[37] Eferl R and Wagner EF. AP-1: a double-edged sword in tumorigenesis. Nat Rev Cancer 2003; 3: 859-868.

[38] Trarallo V, Tudisco L and De Falco S. A placenta growth 2 variant acts as dominant negative of vascular endothelial growth factor a by heterodimerization mechanism. Am J Cancer Res 2011; 1: 265-274.

[39] Huang S, Pettaway CA, Uehara H, Bucana CD and Fidler IJ. Blockade of NF-kappaB activity in human prostate cancer cells is associated with suppression of angiogenesis, invasion, and metastasis. Oncogene 2001; 20: 4188-4197.

[40] Stathopoulos GT, Sherrill TP, Han W, Sadikot RT, Polosukhin VV, Fingleton B, Yull FE and Blackwell TS. Use of bioluminescent imaging to investigate the role of nuclear factor-kappa Beta in experimental non-small cell lung cancer metastasis. Clin Exp Metastasis 2008; 25: 43-51.

[41] Zhu H, Bhaijee F, Ishaq N, Pepper DJ, Backus K, Brown AS, Zhou X and Miele L. Correlation of Notch1, pAKT and nuclear NF-kB expression in triple negative breast cancer. Am J Cancer Res 2013; 3: 230-239.